Chemical Geology 587 (2022) 120625

Contents lists available at ScienceDirect

Chemical Geology

journal homepage: www.elsevier.com/locate/chemgeo

Strontium isotope fractionation during precipitation of strontianite in aqueous solutions as a function of temperature and reaction rate

Mahmoud Alkhatib [a], Mutaz Qutob [a,*], Samia Alkhatib [a], Anton Eisenhauer [b]

[a] Al-Quds University, Jerusalem, Palestinian Authority
[b] GEOMAR Helmholtz-Zentrum für Ozeanforschung Kiel, 24148 Kiel, Wischhofstr. 1-3, Germany

ARTICLE INFO

Editor: Dr Claudia Romano

Keywords:
Strontium isotope
Fractionation
Strontianite precipitation

ABSTRACT

In order to study Strontium (Sr) isotope fractionation during the precipitation of strontianite ($SrCO_3$) as a function of the specific precipitation rate (R*) and temperature (T), strontianite was precipitated at 12.5, 25.0 and 37.5 °C by diffusing NH_3 and CO_2 gases into aqueous solutions. The specific precipitation rate R* (mol/cm^2·h) for every sample was determined by applying the initial rate method. The mean isotope difference between bulk solution and precipitate ($\Delta^{88/86}Sr_{strontianite\text{-}solution}$) was found to be −0.279 ± 0.005‰ ($2\sigma_{mean}$) independent of both rate and temperature. Hence, Sr isotope fractionation in strontianite is completely different from that in calcite and aragonite, where a strong dependency from both rate and temperature can be observed. The latter is interpreted to reflect the competition between Sr^{2+} and Ca^{2+} ions for incorporation into the calcium carbonate crystal lattice, which is absent during the precipitation of pure strontianite. The isotope difference between strontianite and bulk solution then simply reflects the intermolecular forces in the aqueous solutions as well as the kinetic effect. The difference in the ($\Delta^{88/86}Sr_{strontianite\text{-}solution}$ between experiments then reflects the dehydration energy of Sr ions in the adsorption layer of $SrCO_3$.

1. Introduction

Strontium (Sr) is one of the major components of seawater, present in a concentration of 87.4 ± 0.56% μM (De Villiers, 1999). The principal Sr minerals are celestite ($SrSO_4$) and strontianite ($SrCO_3$), the former mineral being more abundant (Martinez and Uribe, 1995) and produced by the marine Radiolaria Acantharia (Odum, 1951). Strontianite is rarely produced in a marine environment, such as in snails (Physa) shells (Odum, 1951) or by cyanobacteria when it is cultured in aqueous solution containing equal concentration of Ca^{2+} and Sr^{2+}ions (Schultze-lam and Beveridge, 1994). Celestite and strontianite are mainly considered impurities that are crystallized during the calcification processes. Strontium coprecipitates with calcium carbonate ($CaCO_3$) polymorphs (aragonite and calcite), and calcium (Ca) coprecipitates with strontianite ($SrCO_3$) (Holland et al., 1963). The mineral or mixture of minerals (aragonite, calcite and/or strontianite) precipitates in accordance with the precipitation conditions (temperature, Mg/Ca and Sr/Ca ratios) of the aqueous solution in which the minerals were deposited. When this ratio is about 0.67, $SrCO_3$ starts to precipitate with aragonite, forming a solid solution, and when the ratio becomes about 0.8, $SrCO_3$ it is formed as a single solid phase (Holland et al., 1963; Plummer and Busenberg, 1987; Greegor et al., 1997). Strontium is present in natural aragonites at higher concentrations (≈ ten times) than in calcite due to the isostructural crystallization of aragonite and strontianite (De Villiers, 1971; Speer, 1983). Foraminifera, for example, are responsible for about 20% of the total calcite sediments and 5 to 10% of the total sediments in the marine environments form the main marine sink of Sr (Böhm et al., 2012; Vollstaedt et al., 2014). The enrichment of strontium in biogenic and inorganic $CaCO_3$ relative to Ca reflects the chemical conditions at their time of formation, conditions such as temperature, salinity and the chemical composition of seawater (AlKhatib and Eisenhauer, 2017a and 2017b; Tang et al., 2008a and 2012). In this regard, Sr/Ca ratios measured in fossil biogenic $CaCO_3$ (corals, foraminifera, etc.) are a suitable archive providing valuable proxy information for oceanographic data, (e.g. Stoll et al., 2002; Gaetani and Cohen, 2006; Gaetani et al., 2011). For example, Sr/Ca ratios are applied as temperature proxy in corals and have been used to reconstruct past sea surface temperatures (SSTs) (c.f. Beck et al., 1992). With respect to biogenic origin, it is also affected by the individual, species- dependent "vital effect" (Elderfield et al., 1996; Lea et al., 1999). It describes the deviation of measured trace elements and isotope ratios from the thermodynamic equilibrium due to the physiological control of the calcifying

* Corresponding author.
E-mail address: kutob@staff.alquds.edu (M. Qutob).

https://doi.org/10.1016/j.chemgeo.2021.120625
Received 6 July 2021; Received in revised form 2 November 2021; Accepted 3 November 2021
Available online 7 November 2021

metabolism on its trace metal uptake. It was also argued, furthermore, that the difference between measured and theoretically predicted values isdue to the simultaneous presence of $SrCO_3$ in the $CaCO_3$ lattice (Greegor et al., 1997) due to the coprecipitation of $SrCO_3$ with aragonite. Multiple studies have been conducted on the effect of precipitation rate R* and temperature on Sr enrichment and isotopic fractionation during the precipitation of calcite and aragonite (e.g. Tang et al., 2008a, 2008b; Böhm et al., 2012 and AlKhatib and Eisenhauer, 2017a and 2017b). In general, all of these studies demonstrated a direct relationship between precipitation rate R* and both the enrichment of Sr and the extent of its isotopic fractionation toward lighter Sr isotopes incorporated in $CaCO_3$. In contrast to the precipitation rate R*, increasing temperature decreased the enrichment of Sr in $CaCO_3$ and also decreased the extent of Sr isotopic fractionation toward lighter Sr isotopes. While the rate R* effect is more important in calcite precipitation, temperature effect, by contrast, is more significant in aragonite precipitation. In contrast to Ca, neither D_{Sr} nor $\Delta^{88/86}Sr_{calcite\ -\ aq}$ and $\Delta^{88/86}Sr_{aragonite\ -\ aq}$ depend on the type of bonding in the solution (AlKhatib and Eisenhauer, 2017a and 2017b). In fact, it is not only the precipitation rate and temperature that are responsible for Sr enrichment and isotope fractionation in $CaCO_3$, but also the competition with other ions such as Mg^{2+} and Ca^{2+} to become incorporated into $CaCO_3$ (AlKhatib and Eisenhauer, 2017b). The uptake of ions from the aqueous solution depends on their relative abundance in an aqueous solution, and the dehydration energy needed to release each ion from its aqua complex is inversely related to its ionic radii. Of the three ions, Sr^{2+} (116 pm) has the lower dehydration energy (1443 kJ/mol) and Mg^{2+} (72 pm) has the highest dehydration energy (1921 kJ/mol) (Atkins and De Paulla, 2006; Irving and Williams, 1953). Ion enrichment also depends on the extent to which each ion fits well in the $CaCO_3$ lattice. Magnesium fits well in calcite but not into aragonite crystal lattice (Kelleher and Redfern, 2002; Meibom et al., 2004). It was found that Mg distribution in aragonite (D_{Mg}) increases with precipitation rate R* and decreases with increasing temperature. In general, it is about three orders of magnitude lower than D_{Sr} in aragonite (AlKhatib and Eisenhauer, 2017b). The solutions from which aragonite can be precipitated must have a high Mg/Ca ratio (3 or more) and due to the lower value of D_{Mg}, Mg is not thought to become incorporated into the aragonite lattice. Rather, it is adsorbed only on the surface, creating what is called the "Mg blocking effect," which interferes with both Sr enrichment and Sr isotope fractionation in aragonite (AlKhatib and Eisenhauer, 2017b). The "Mg blocking effect" increases the solubility of crystals and enhances the release of crystal lattice bound isotopically light Sr. The "Mg blocking effect" is diminished as a function of rising temperatures, less Mg is adsorbed on the aragonite crystal surface, and relatively more Ca from the fluid is incorporated.

Studies on Sr isotope fractionation during $SrCO_3$ precipitation are rare. Recently, Mavromatis et al., 2017) studied Sr isotope fractionation during $SrCO_3$ dissolution and precipitation, showing that isotope exchange between solid $SrCO_3$ and Sr^{2+} ions in an aqueous solution still continuous despite the achievement of a chemical equilibrium. Recent research findings very surprisingly challenge the applicability of Sr isotopes as an environmental proxy. In addition, precipitation of strontianite as pure crystals along with $CaCO_3$ may also affect its use as a proxy To avoid this complexity, it is important to see how Sr isotopic composition in strontianite vary with temperature and precipitation rate.

In order to examine the influence and interference of Sr partitioning and isotope fractionation in $SrCO_3$ during co-precipitation with $CaCO_3$, we performed $SrCO_3$ precipitation experiments at different R* values and temperatures (12.5, 25 and 37.5 °C).

2. Material and methods

2.1. Materials and experimental setup

The original experimental setup of this method of precipitating $SrCO_3$ as shown in Fig. 1 was described earlier by AlKhatib and Eisenhauer (2017a, 2017b) to precipitate calcite and aragonite. $SrCO_3$ was prepared in an ammonium buffered solution (NH_4/NH_3) at three different temperatures 12.5, 25.0 and 37.5 (±0.2 °C). The reacting solution was composed of 0.395 M NH_4Cl and 10, 15 and 20 mM $SrCl_2$. NH_4Cl was used here to buffer the solution and adjust the ionic strength of the solutions. All of the chemicals were ACS grade of Merck and all aqueous solutions were prepared using deionized water (18.2 MΩ). In this technique, 400 ml of NH_4Cl-$SrCl_2$- solution and the solid $(NH_4)_2CO_3$ (ammonium carbonate) was contained within the sealed reacting chamber (see Fig. 1). In all experiments, the reacting solution is stirred with a magnetic stirrer at 300 rounds per minute. Ammonium carbonate decomposes spontaneously and produces an ammonia /carbon dioxide atmosphere within the chamber by the reaction:

(1) $(NH_4)_2CO_{3\ (S)} \leftrightarrow 2NH_{3\ (g)} + CO_{2\ (g)} + H_2O_{\ (g)}$

Ammonia and carbon dioxide gases diffuse and dissolve in the experimental solution increasing pH and alkalinity by the following reactions:

(2) $NH_{3(g)} + H_2O \rightleftharpoons NH_4^{+}{}_{(aq)} + OH^{-}{}_{(aq)}$
(3) $CO_{2(g)} + H_2O \rightleftharpoons CO_{2(aq)}$
(4) $CO_{2(aq)} + H_2O \rightleftharpoons H_2CO_3$
(5) $H_2CO_3 \rightleftharpoons HCO_3^{-}{}_{(aq)} + H^{+}{}_{(aq)}$
(6) $HCO_3^{-}{}_{(aq)} \rightleftharpoons CO_3^{-}{}_{(aq)} + H^{+}{}_{(aq)}$

The overall spontaneous reaction of the steps (1) to (6) is:
$(NH_4)_2CO_3\ (s) \rightarrow 2NH_4^{+}\ (aq) + CO_3^{2-}\ (aq)$

The result was the supersaturation of the reacting solution with respect to strontianite. The reaction dynamics was monitored by a WTW 3100 pH meter, which was standardized against buffer solutions of pH 4, 7 and 10 before each experiment. This pH meter connected to a computer that continuously monitors the pH values and the temperature of the solution online and stores the measured data on an Excel sheet. We controlled the rate of reaction as well as the time needed to reach the precipitation point by the quantity, the surface area of the granules of ammonium carbonate, and by the surface area through which the gases diffuse. During the experiment, the chemical evolution of the reacting solution was monitored by sampling 2 to 5 ml at distinct time intervals, ranging between 5 and 30 min, depending on the reaction time to be analyzed later. We allowed each reaction to run for a certain period of time, depending on its rate, and then stopped it by removing the reacting solution from the sealed chamber and filtering the solution as quickly as possible by vacuum filtration through a regenerated cellulose filter paper with a pore size of 0.2 μm. Then the solid was then washed with deionized water (18.2 MΩ) and mixed with a small volume of pure ammonium hydroxide solution to make it slightly alkaline. Finally, the filter was washed with pure ethanol in order to remove any adsorbed $SrCl_2$ aqueous solutions on the surface of the crystals.

2.2. Analysis

2.2.1. Dissolved inorganic carbon (DIC)

In order to calculate the DIC, the total alkalinity (TA) of each experiment over the entire period of reaction has to be calculated. We did this by titrating 0.2 ml of the reaction mixture at different intervals of time during the precipitation reaction against 0.002 N HCl (dilution of MERCK-Titrisol-solution™). This HCl solution is initially standardized against IAPSO seawater (Certified alkalinity of 2.325 mM) using a micro titration apparatus Metrohm 665 Dosimat equipped with a titration

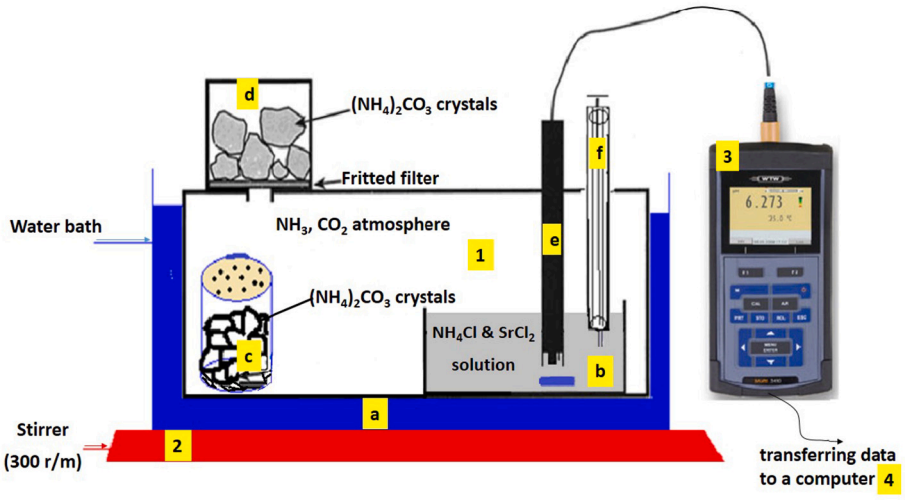

Fig. 1. schematic design of the experimental setup: (**1**) the reaction chamber which is a sealed plastic container consisting of a copper tubing (**a**) where water is circulating to keep a constant temperature, (**b**) beaker that contains the reacting solution, (**c**) a beaker that contains some ammonium carbonate granules that decompose spontaneously to provide ammonia and carbon dioxide gases, (**d**) fritted filter funnel that also contains some ammonium carbonate granules, (**e**) pH and temperature sensors, (**f**) syringe to withdraw samples from the reacting solution, (**2**) magnetic stirrer, (**3**) pH meter and (**4**) computer recording the measured data in an excel sheet (AlKhatib and Eisenhauer, 2017).

vessel of 7 cm height. During the titration, the sample is continuously degassed with nitrogen to remove any CO_2. A mixed indicator solution (methyl red/methylene blue) was used in this titration. Each sample was titrated three times and the average volume was used to calculate the total alkalinity. Details regarding the [DIC] in our system has been described earlier in AlKhatib and Eisenhauer (2017a).

2.2.2. Elemental analysis

We analyzed the concentration of Sr ions in the bulk solutions at different intervals of time during the course of each reaction to calculate the precipitation rate of each single sample reaction by inductively coupled plasma mass spectrometry (ICP-MS-QP Agilent 7500cx) together with Indium (In) as an internal standard.

2.2.3. Crystalline structure of strontianite products

The crystalline structure of the solid products was performed with an X-Ray-diffractometer "D8 Discover" (Bruker AXS). The samples were analyzed in a 2Θ-range from 4° to 90°, with a step size of 0.007° and counting time of 1.5 s/step using a Cu X-ray radiation source. The software was evaluated by High Score Plus Version 3.0d (3.0.4) by PANalytical. All measurements were carried out at the Geology Department of Kiel University. All samples were determined to be pure strontianite.

2.2.4. Specific surface area of strontianite products

The specific surface area of the final $SrCO_3$ products was determined by applying the Brunauer Emmett- Teller (BET) gas adsorption method (De Kanel and Morse, 1979) using "BET FLOWSORB II 2300" at 22.6 °C and 968 mbar. Of the total number of 22 $SrCO_3$ samples produced in this study, we analyzed 11 having enough material (at least 100 mg) necessary for analysis by the BET method. The measurements were carried out at the University of Graz, Austria.

2.2.5. Strontium and calcium isotope analysis

Measurements were carried out at the GEOMAR mass spectrometer facilities in Kiel, Germany, using a ThermoFisher Triton T1 Thermal-Ionization-Mass-Spectrometer (TIMS). Strontium ($\delta^{88/86}Sr$) isotope composition was measured for all solid products as well as for the starting solution of these reactions, closely following the procedure described earlier by (Krabbenhöft et al., 2009). At least two isotope measurements had to be performed, one unspiked run (ic-run, isotope composition) and one run with a $^{87}Sr/^{84}Sr$-double spike added to the sample solution (id-run, isotope dilution). Sample size was determined to be in the order of 1500 ng of Sr. Spike correction and normalization of the results were carried out in a manner described by (Krabbenhöft et al., 2009). During the course of this procedure, two ic-run and id-run for each sample in each session were measured. The measured $^{88}Sr/^{86}Sr$ ratios are reported in the common δ-notation relative to NIST SRM987: $\delta^{88/86}Sr\ (‰) = [(^{88}Sr/^{86}Sr)_{sample}/(^{88}Sr/^{86}Sr)_{SRM987}-1]$.

We are reporting Sr fractionation in the big delta notations $\Delta^{88/86}Sr = \delta^{88/86}Sr_{strontianite} - \delta^{88/86}Sr_{initial}$ solution. All Δ-values are corrected for Rayleigh distillation effect in order to account for the reservoir effect, as shown in Eq. (7) derived by AlKhatib and Eisenhauer (2017a).

$$(7)\quad \alpha_{corrected} = \left(ln\left[\frac{\Delta f}{1000} + f - \left(\frac{\Delta}{1000}\right)\right]\right) \Big/ lnf$$

Where f is the fraction of Sr^{2+} ions remaining in the aqueous solution and α is the isotope fractionation factor defined as $(^{88}Sr/^{86}Sr_{strontianite}/^{88}Sr/^{86}Sr_{initial\ solution})$.

$$(8)\quad \Delta corrected \approx (\alpha_{corrected} - 1) \bullet 1000$$

In Table 1, the original data together with the corrected data for Rayleigh fractionation are presented. In Table 2, Temperature (T), pH, total alkalinity, initial and final concentration of Sr, running time of reaction, concentration of ammonia, dissolved inorganic carbon (DIC), carbonate ions concentration, saturation index (SI), rate are presented.

3. Results

3.1. pH, total alkalinity (TA) and dissolved inorganic carbon (DIC)

The experiment shows that the pH of the solution gradually increases as soon as the absorption of the evolved gases (CO_2 and NH_3) into aqueous solution starts and continues until it reaches a maximum value. It decreases slightly after the start of precipitation. The Sr^{2+} – ions react with HCO_3^- but then are redistributed to $CO_3^{2,}$ which, according to Eq. (9), results in a pH drop. The start of precipitation is also characterized by a drop in dissolved strontium (Sr) in the solution exactly at this pH.

Table 1
$[Sr^{2+}]$ variation as function of time of sample reaction 10 at 12.5 °C.

Time/h	$[Sr^{2+}]$ /mM
0.0	9.54
0.33	9.29
0.62	9.03
1.08	8.65
1.33	8.50

Table 2
Temperature (T), pH, total alkalinity, initial and final concentration of Sr, running time of reaction, concentration of ammonia, dissolved inorganic carbon (DIC), carbonate ions concentration, saturation index (SI), rate.

Sample reaction	Temperature °C±0.2	pH	Total alkalinity mM±0.02	Initial [Sr] concentration mM±0.01	Final [Sr] concentration mM±0.01	Experiment running time/ minutes	[NH_3]/ mM	[DIC]/ mM	[CO_3^{2-}] mM	SI of $SrCO_3$	Rate (mM/ h)	±(2SEM)	R* (μ mol/m^{2}h)	log R*	Uncorrected $\Delta^{88/86}$Sr‰	Corrected $\Delta^{88/86}$Sr ‰	±(2SEM)
1	2	3	4	5	6	7	8	9	10	11	12	13	14	15	16	17	18
1	25.0	8.095	16.61	9.85	6.49	167	15.66	0.95	0.104	3.291	1.21	0.29	2159	3.33	-0.217	-0.270	0.004
2	25.0	8.029	14.03	19.51	16.80	185	13.44	0.59	0.059	3.342	0.88	0.32	1947	3.29	-0.257	-0.277	0.007
3	25.0	8.064	16.84	9.82	6.46	58	14.63	2.21	0.228	3.631	3.48	0.84	6209	3.79	-0.231	-0.287	0.003
4	25.0	8.109	17.29	19.64	15.29	239	16.18	1.11	0.127	3.678	1.09	0.17	1502	3.18	-0.232	-0.263	0.004
5	25.0	8.002	14.26	19.48	17.30	39	12.66	1.60	0.151	3.749	3.36	0.39	9239	3.97	-0.275	-0.291	0.008
6	25.0	7.919	12.13	14.47	12.39	40	10.58	1.55	0.123	3.531	3.12	0.45	8992	3.95	-0.257	-0.277	0.003
7	25.0	8.011	15.24	9.61	6.78	39	12.95	2.29	0.211	3.588	4.39	0.19	9299	3.97	-0.233	-0.278	0.006
8	25.0	7.970	13.27	19.40	16.91	52	11.76	1.51	0.134	3.696	2.90	0.57	6981	3.84	-0.257	-0.276	0.007
9	12.5	8.221	9.28	9.54	8.50	78	8.64	0.64	0.051	2.958	0.80	0.07	4611	3.66	-0.242	-0.257	0.003
10	12.5	7.816	4.69	14.67	13.22	60	3.37	1.32	0.046	3.100	1.46	0.51	6036	3.78	-0.244	-0.258	0.003
11	12.5	8.050	9.32	10.15	7.65	23	5.87	3.45	0.196	3.570	6.48	0.22	15538	4.19	-0.241	-0.278	0.005
12	12.5	7.849	5.88	20.24	18.30	24	3.65	2.23	0.086	3.512	4.92	0.25	15202	4.18	-0.268	-0.282	0.004
13	12.5	8.145	9.28	10.13	7.28	96	7.27	2.01	0.138	3.416	1.78	0.25	3744	3.57	-0.249	-0.295	0.004
14	12.5	8.060	6.84	20.04	18.64	66	5.96	0.88	0.052	3.289	1.28	0.34	5481	3.74	-0.280	-0.291	0.004
15	37.5	7.892	26.18	10.33	5.05	169	22.52	3.66	0.347	3.857	1.87	0.11	2123	3.33	-0.198	-0.289	0.005
16	37.5	7.832	23.05	20.09	15.32	143	19.61	3.44	0.300	4.083	2.00	0.05	2513	3.40	-0.258	-0.296	0.002
17	37.5	7.480	15.63	10.39	7.75	72	8.89	6.74	0.280	3.767	2.20	0.07	4995	3.70	-0.253	-0.294	0.005
18	37.5	7.380	11.14	20.29	17.88	44	7.02	4.12	0.143	3.765	3.25	0.08	8084	3.91	-0.258	-0.279	0.003
19	37.5	7.529	27.31	15.05	11.15	27	10.11	17.20	0.805	4.386	8.79	0.67	13510	4.13	-0.260	-0.304	0.004
20	37.5	7.652	27.30	15.18	10.98	37	13.44	13.86	0.835	4.406	6.80	0.54	9705	3.99	-0.234	-0.276	0.002
21	37.5	7.422	9.05	10.95	8.76	337	7.67	1.38	0.051	3.050	0.39	0.20	1067	3.03	-0.232	-0.260	0.010
22	37.5	7.320	6.80	20.63	19.04	222	6.00	0.80	0.024	2.997	0.43	0.20	1621	3.21	-0.255	-0.265	0.002

(R), normalized rate to the surface area (R*), log R*, $\Delta^{88/86}$ Sr (‰) uncorrected and corrected values.

Notes: TA was measured from titrating the final solution with HCl, pH measured at the end of each reaction, initial and final [Sr] measured by ICP-MS, [NH_3], [DIC], [CO_3^{2-}] and SI of $SrCO_3$ were calculated from equations 11, 10, 13 and 15 respectively, For all reactions rate (mM/h) was calculated as explained in the text and fig.2 a. R* is calculated according to equation 16 in the text. **Column 1**6 shows the measured isotope values of Sr uncorrected for the reservoir effect. **Column 1**7 is the corrected values of columns **16** using equations 7 and 8 in the text.

(9) $HCO_3^- + Sr^{2+} \rightleftharpoons SrCO_{3(S)} + H^+$

Throughout the reaction, the pH of the reacting solution (when precipitation starts) remains relatively constant (±0.02 units) as does the temperature of all reactions (±0.2 °C). Total alkalinity (TA) was measured from neutralization titration with 0.002 N HCl at different intervals of time during the course of precipitation for some reactions. We found that TA did not increase more than 10% from the value at the precipitation point to the end of the reaction. We therefore determined TA at the end of all the reactions and adopted this value for further calculations.

(10) $TA = [NH_3] + [HCO_3^-] + 2[CO_3^{2-}]$

$[NH_3]$ in our solutions at different results is calculated following Lemarchand et al. (2004):

(11) $$[NH_3] = \frac{[Cl^-] + TA - 2[Sr^{2+}]}{\frac{[H^+]}{K_a} + 1}$$

where $[Sr^{2+}]$ is the initial concentration of strontium ions in the solution $[Cl^-]$ is the concentration of chloride ions, $[H^+]$ calculated from pH values at the end of each experiment and K_a ($pK_a = -\log K_a$) is the ammonium acid dissociation constant, which is temperature- dependent and can be calculated using Eq. (12), following AlKhatib and Eisenhauer (2017a).

(12) $pK_a = 2651.4/T + 0.60$

Where T is the temperature in degree Kelvin. The results are summarized in Table 1.

3.2. Precipitation rate

Plotting the concentration of Sr ions in the bulk solutions versus time during the course of each reaction allows for the calculation of the precipitation rate of each single sample reaction. As shown in Fig. 2 of randomly selected sample reaction 9, the slope of the linear relationship equals the precipitation rate (0.80 mM/h). From Fig. 3 it can be seen that the determined specific surface areas (S) of strontianite products scatter to a large extent. Given the limited number of points, it is not easy to see the dependence of S on temperature and R.

Hence, it can be assumed that S of all strontianite products is equal to an average value of 1.13 ± 0.27 m^2/g or equivalent to 166.82 ± 39.86 m^2/mol. The latter value is very close to that of the surface area of $SrCO_3$ (1.1 ± 0.1 m^2/g) produced earlier by Mavromatis et al. (2017). From this value, the normalized rate of reaction R* (μmol/m^2·h) is calculated using Eq. (13) (AlKhatib and Eisenhauer, 2017a).

(13) $$R^* = \frac{\text{initial rate (mM/h) x volume of reacting solution (ml)}}{\text{Area of } SrCO_3(m^2)}$$

where the value of the numerator equals the initial rate (μmol/h) and the total area of $SrCO_3$ in each sample reaction equals the moles of $SrCO_3$ produced at the end of each experiment multiplied by the specific surface area of strontianite S. The results are summarized in Table 1.

3.3. Sr isotope fractionation measurements

The average $\delta^{88/86}Sr$ value of the initial Sr solution is determined to be 0.165 ± 0.002‰ ($n = 4$) It is similar to the reacting solution used to precipitate $SrCO_3$ in Mavromatis et al. (2017) $\delta^{88/86}Sr$ 0.154 ± 0.013‰. It can be seen from Fig. 4 and Table 1 that Sr isotopic composition in strontianite is fractionated with a constant value and that $\Delta^{88/86}Sr$ values are independent of both precipitation rate and temperature. The average corrected value for the reservoir effect $\Delta^{88/86}Sr_{strontianite\text{-}solution}$ = −0.279 ± 0.005‰ ($2\sigma_{mean}$). On the other hand, Mavromatis et al. (2017) calculated $\Delta^{88/86}Sr_{strontianite\text{-}solution} = -0.15$‰, depending on the measurement of the instant $\delta^{88/86}Sr_{fluid}$ during the precipitation process of $SrCO_3$ and suggesting a mechanism of Sr^{2+} ion exchange between the

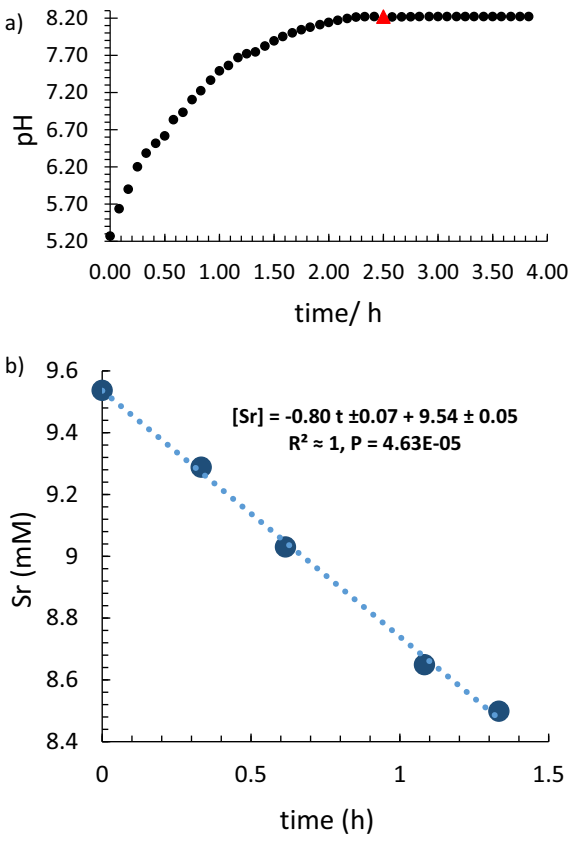

Fig. 2. a. The pH variations of solution versus time of sample reaction 10 at 12.5 °C. The saturation point (the point at which precipitation starts) is presented as a red triangle (2.5, 8.221). **b.** Changes of Sr^{2+}-ion concentration as function of time for arbitrarily selected sample reaction 10 to produce strontianite at 12.5 °C. The slope of the linear relationship equals the precipitation rate. (For interpretation of the references to colour in this figure legend, the reader is referred to the web version of this article.)

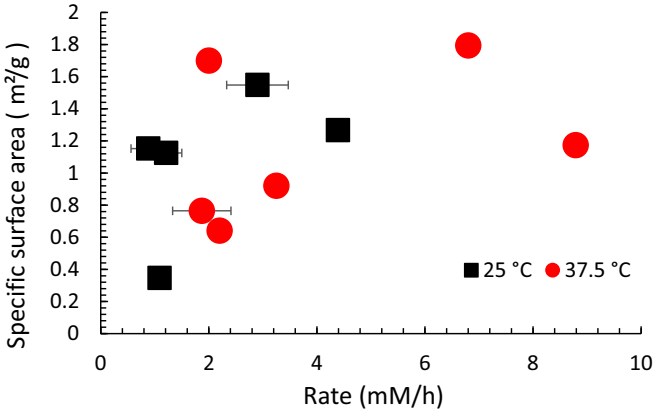

Fig. 3. Specific surface area (S) determined by the BET method (BET = Brunauer-Emmett-Teller gas adsorption method) of some strontianite precipitates versus precipitation rate (R, mM/h) at different temperatures. The value of S is independent of both temperature and precipitation rate and equal to the average value 1.13 ± 0.27 m^2/g.

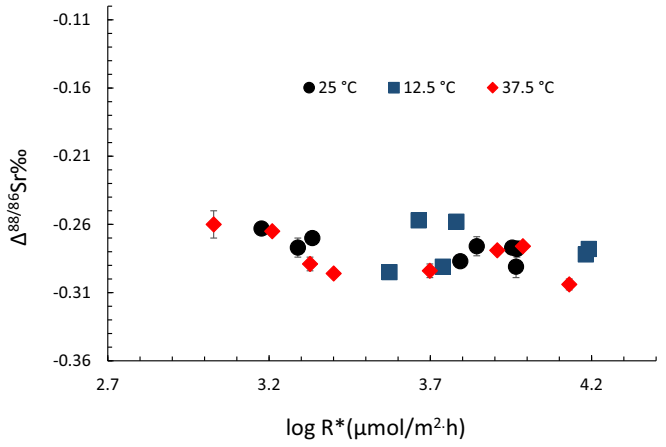

Fig. 4. This diagram shows all $\Delta^{88/86}Sr_{strontianite\text{-}aq}$ values as a function of their corresponding log R*(μmol/m^2·h) data for all temperatures. It can be seen that $\Delta^{88/86}$Sr‰ values are independent of both precipitation rate and temperature. The average value of $\Delta^{88/86}$Sr‰ = −0.279 ± 0.005 (± is $2\sigma_{mean}$).

fluid and crystal interior, rather than just with the surface.

4. Discussion

One of the most important factors affecting trace elements enrichment and isotope fractionation is the competition with other metal ions to be incorporated into $CaCO_3$. There is a strong, direct correlation between Sr enrichment in $CaCO_3$ (calcite and aragonite), described as Sr partitioning coefficient (D_{Sr}) and Sr isotope fractionation $\Delta^{88/86}Sr_{CaCO3\text{-}solution}$ (Böhm et al., 2012; AlKhatib and Eisenhauer, 2017a and 2017b). The surface crystal at any moment of crystal growth will be enriched relatively higher with Sr^{2+} over Ca^{2+} ions This depends largely on the dehydration energy of ions. Dehydration energy actually depends on the ionic radii, for Ca^{2+} (100 pm) to be 1577 kJ/mol and of Sr^{2+} (116 pm) to be 1443 kJ/mol (Irving and Williams, 1953; Rodriguez-Cruz et al., 1999). Not only will the surface be enriched with Sr^{2+} ions but also with lighter Sr isotopes (Watson, 2004; Böhm et al., 2012) because lighter Sr isotopes possess more kinetic energy than heavier isotopes to overcome the activation energy of dehydration. Subsequent events that take place during crystal growth are responsible for both Sr enrichment and Sr isotope fractionation. Nevertheless, the relatively larger ratio of Sr^{2+} ions have been adsorbed at the crystal surface. Nevertheless, Ca^{2+} ions are preferentially incorporated into $CaCO_3$ because the Ca^{2+} ion radius fits perfectly well into the $CaCO_3$ lattice, in contrast to Sr^{2+} ion (Blundy and Wood, 2003). This sort of competition between different types of ions will create a difference in the chemical composition between the bulk crystal and surface crystal. The disequilibrium state between bulk crystal and crystal surface will induce diffusion (desorption) of Sr^{2+} ions back to the near surface region of the growing crystal, aspiring to reach a new equilibrium state (Watson, 2004).

Of course, the diffused (desorbed) Sr^{2+} ions will be richer in lighter isotopes, keeping Sr isotope composition in the bulk crystal heavier, but still lighter than the bulk solution. As result, the extent to which Sr desorbed from the surface crystal back to the bulk solution will control both Sr enrichment and Sr isotope fractionation in the final bulk solid. More diffusivity (desorption) will produce $CaCO_3$ with less Sr incorporated into it and with less Sr isotope fractionation (less negative $\Delta^{88/86}Sr_{CaCO3\text{-}solution}$ values).

Diffusivity will stop when Sr^{2+} ions become entrapped (captured) under the surface crystal and are no longer in contact with the fluid. At very low precipitation rates and at relatively high temperatures, the rate of desorption is relatively high and almost equal to the rate of accumulation (adsorption) of Sr^{2+} ions (approaching equilibrium). Increasing the precipitation rate will increase the entrapment of more Sr^{2+} ion to the surface crystal especially with lighter Sr isotope composition.

Here, diffusivity becomes unable to desorb the entrapped Sr^{2+} ions efficiently as when the precipitation rate was low, since more Sr^{2+} ions will be imbedded down the crystal surface and are no longer in contact with the fluid. As a result, more Sr will be incorporated into $CaCO_3$ with more isotopic fractionation (more negative $\Delta^{88/86}Sr_{CaCO3\text{-}solution}$ values). The effect of decreasing temperature is equivalent to the effect of the increasing precipitation rate. Since a decreasing temperature will reduce the mobility of ions and as result reduce the diffusivity of Sr^{2+} ions toward aqueous solution, the rate of adsorption will again overcome the rate of desorption of Sr^{2+} ions. This explanation is in fact consistent with the results of previous work by AlKhatib and Eisenhauer, 2017a and 2017b) as shown in Fig. 4. As the rate of precipitation increase more lighter Sr isotopes are incorporated into $CaCO_3$, corresponding to decreasing $\Delta^{88/86}Sr_{CaCO3\text{–}aq}$ values. As temperature increases, $\Delta^{88/86}$Sr values become more positive at the same R*. The difference between calcite and aragonite is that the R*- $\Delta^{88/86}Sr_{calcite\text{-}aq}$ gradients are much steeper for calcite than for aragonite and at the same isotope values, the calcite precipitation rate is higher than that of aragonite.

This difference is attributed to the additional competition of Mg^{2+} ions that adsorbed largely at the surface crystal, thereby increasing the solubility of crystal, reducing the precipitation rate R*, and inducing more diffusivity of Sr^{2+} ions back to the bulk solution. As result, it decreases the effect of precipitation rate on Sr isotope fractionation.

The properties of aqueous electrolyte solutions depend largely on the interaction of ions with the molecules of the water or to to the extent to which they are hydrated and the ease with which these ions can shed their hydration sphere in the adsorption layer and react with other ions to form solid products. The extent of hydration or the stability of the hydrated ions and the ease of dehydration depends on the chemistry of the solution (ionic strength, types of other ions present of the aqueous solution, the presence of other molecular species that can form complexes with metal ions as ammonia, for example), temperature, and the size and the charge of the metal cation.

hThese interactions (hydration, dehydration and the ability to form molecular complexes with metal cations) are extremely important for the equilibrium properties of solutions (e.g. vapor pressure and boiling point), properties that are known as kinetic properties (viscosity, electrical conductivity, mobility and their diffusion coefficient of ions) (Atkins and De Paulla, 2006) and for the isotope fractionation of different atoms during the precipitation from aqueous solutions. Since Ca^{2+} ion (radius 100 pm) is smaller than other alkaline earth elements, Sr^{2+} (116 pm) and Ba^{2+} (136 pm), its dehydration energy is relatively large, 1577 kJ/mol, and the fraction of lighter Ca isotopes which possess enough kinetic energy to overcome aqua complex and is able to react to form $CaCO_3$ is largely dependent on precipitation rate and temperature. Ca isotope fraction is not only dependent on rate and temperature but also on the chemistry of the aqueous solution. This was responsible for the discrepancy of the dependency of Ca isotope fractionation on precipitation rate between different experimental results in the literature (Lemarchand et al., 2004; Tang et al., 2008b; AlKhatib and Eisenhauer, 2017a, 2017b).

This discrepancy is attributed to the ability of forming relatively stable Ca^{2+}-NH_3 complex versus Ca^{2+}-H_2O aqua complex depending on the composition of the aqueous solution and the temperature of the reaction (AlKhatib and Eisenhauer, 2017a, 2017b). In contrast to Sr and Ca in $CaCO_3$, Sr in strontianite is fractionated at a constant value independent of temperature and rate R* and we expect that this result is due to the absence of the two main factors which are responsible for isotope fractionation. The first is the absence of the competition with other metal cation (Ca^{2+} and Mg^{2+}) to precipitate in strontianite pure crystals. The surface crystal and the bulk crystal always have the same chemical composition and are in equilibrium with each other. As result, we expect a very limited chemical desorption (breaking of ionic bonds of Sr^{2+} ions at the surface crystal).

The second reason is due to the relatively larger Sr^{+2} radius (116 pm). Unlike Ca, it is impossible for Sr^{2+} ions to form neither the relatively stable Sr^{2+}-NH_3 complex nor the Sr^{2+}-H_2O aqua complex. Sr is only fractionated due to the ease with which lighter Sr isotdopes shed (get rid of) their hydration sphere at the solid interphase because they possess more kinetic energy than the heavier one. Consequently, Sr will be fractionated at a constant value independently of precipitation rate and temperature, showing a thermodynamic isotopic fractionation (Watson, 2004) which is consistent with our experimental results as shown in in Fig. (4 and 5) and Table 1.

Although it is impossible for Sr^{2+} ions to form relatively stable molecular complexes, the chemistry (the composition) of aqueous solutions can still affect the extent of Sr isotope composition by affecting the physical properties of the aqueous solution. The addition of ions will create ion-dipole interaction and the addition of ammonia will create an increase in hydrogen bonds with water molecules. These additional intermolecular forces depend on the concentration of added species. As the concentration increases, the intermolecular forces between water molecules increases. This will cause a decrease in the vapor pressure of water, an increase in the boiling point of aqueous solution, decreasing the partial molar volume of water, increasing viscosity, which will decrease the mobility and diffusion coefficient of ions in aqueous solutions, and of course increase the activation energy of dehydration of the reacting ions (Atkins and De Paulla, 2006), and only lighter Sr isotopes will possess enough activation energy for dehydration. As a result, we expect that the strontianite produced under these conditions will be more fractionated and contain lighter Sr isotopes in the solid and $\Delta^{88/86}Sr_{strontianite\text{-}solution}$ will be more negative. This in fact explains why our value of $\Delta^{88/86}Sr_{strontianite\text{-}solution}$ (−0.279‰) is about the double of what Mavromatis et al. (2017) calculated $\Delta^{88/86}Sr_{strontianite\text{-}solution} = -0.15‰$. They had sed 0.01 M NaCl aqueous solution to precipitate strontianite, while in the present study, strontianite was precipitated from an aqueous solution containing 0.395 M NH_4Cl and at least 3.4 mM NH_3 (Table 1). Thus, the results call for additional strontianite precipitation experiments at different ionic strengths to see how it will affect $\Delta^{88/86}Sr_{strontianite\text{-}solution}$ and to determine if Sr isotope fractionation can be used as a tool to determine the activation energy of dehydration.

5. Implications

The most important implications of the results of this study are as follows

- The co-precipitation of $SrCO_3$ with $CaCO_3$ may not influence their isotope ratios because Sr isotope fractionation in $SrCO_3$ is independent of R* and T.
- Sr isotopic composition in strontianite cannot be used as an environmental proxy because Sr isotope values are independent of both R* rate and T.

Declaration of Competing Interest

The authors declare that they have no known competing financial interests or personal relationships that could have appeared to influence the work reported in this paper.

References

AlKhatib, M., Eisenhauer, A., 2017a. Calcium and strontium isotope fractionation in aqueous solutions as a function of temperature and reaction rate; I. Calcite. Geochim. Cosmochim. Acta 209, 296–319.

AlKhatib, M., Eisenhauer, A., 2017b. Calcium and strontium isotope fractionation during precipitation from aqueous solutions as a function of temperature and reaction rate; II. Aragonite. Geochim. Cosmochim. Acta 209, 320–342.

Atkins, P., De Paulla, J., 2006. Atkins, Physical Chemistry.8th Edition. W.H. Freeman and company, New York, p. 798.

Beck, J.W., Edwards, R.L., Ito, E., Taylor, F., Recy, J., Rougerie, F., Joannot, P., Henin, C., 1992. Sea-surface temperature from coral skeletal strontium calcium ratios. Science 257 (5070), 644–647.

Blundy, J., Wood, B., 2003. Partitioning of trace elements between crystals and melts. Earth Planet. Sci. Lett. 6607, 1–15.

Böhm, F., Eisenhauer, A., Tang, J., Dietzel, M., Krabbenhöft, A., Kisakürek, B., Horn, C., 2012. Strontium isotope fractionation of planktic foraminifera and inorganic calcite. Geochim. Cosmochim. Acta 93, 300–314.

De Kanel, J., Morse, J.W., 1979. A simple technique for surface area determination. J. Phys. E: Sci. Instrum. 12, 272–273.

De Villiers, S., 1999. Seawater strontium and Sr/Ca variability in the Atlantic and Pacific oceans. Earth Planet. Sci. Lett. 171, 623–634.

De Villliers, J.P.R., 1971. Crystal structures of aragonite, strontianite and witherite. Am. Mineral. 56, 758–767.

Elderfield, H., Bertram, C.J., Erez, J., 1996. A biomineralization model for the incorporation of trace elements into foraminiferal calcium carbonate. Earth Planet. Sci. Lett. 142, 409–423.

Gaetani, G.A., Cohen, A.L., 2006. Element partitioning during precipitation of aragonite from seawater: a framework for understanding paleoproxies. Geochim. Cosmochim. Acta 70, 4617–4634.

Gaetani, G.A., Cohen, A.L., Wang, Z., Crusius, J., 2011. Rayleigh-based, multi-element coral thermometry: a biomineralization approach to developing climate proxies. Geochim. Cosmochim. Acta 75, 1920–1932.

Greegor, R.B., Pingitore Jr., N.E., Lytle, F.W., 1997. Strontianite in coral skeletal aragonite. Science 275, 1452–1454.

Holland, H.D., Borcsik, M., MuNozt, J., Oxburghs, U.M., 1963. The coprecipitation of Sr^{+2} with aragonite and of Ca^{+2} with strontianite between 90° and l00°C. Geochim. Cosmochim. Acta 27, 957–977.

Irving, H., Williams, R.J.P., 1953. The stability of transition metal complexes. J. Chem. Soc. 3192–3210.

Kelleher, I.J., Redfern, S.A.T., 2002. Hydrous calcium magnesium carbonate, a possible precursor to the formation of sedimentary dolomite. Mol. Simul. 28 (6–7), 557–572.

Krabbenhöft, A., Fietzke, J., Eisenhauer, A., Liebetrau, V., Böhm, F., Vollstaedt, H., 2009. Determination of radiogenic and stable strontium isotope ratios (87Sr/86Sr; d88/86Sr) by thermal ionization mass spectrometry applying an 87Sr/84Sr double spike. J. Anal. At. Spectrom. 24, 1267–1271.

Lea, D.W., Mashiotta, T.A., Spero, H.J., 1999. Controls on magnesium and strontium uptake in planktonic foraminifera determined by live culturing. Geochim. Cosmochim. Acta 63, 2369–2379.

Lemarchand, D., Wasserburg, G.J., Papanastassiou, D.A., 2004. Rate-controlled calcium isotope fractionation in synthetic calcite. Geochim. Cosmochim. Acta 68, 4665–4678.

Martinez, A.L., Uribe, A.S., 1995. Interfacial properties of celestite and strontianite in aqueous solutions. Min. Eng. 8 (9), 1009–1022.

Mavromatis, V., Harrison, A.L., Eisenhauer, A., Dietzel, M., 2017. Strontium isotope fractionation during strontianite ($SrCO_3$) dissolution, precipitation and at equilibrium. Geochim. Cosmochim. Acta 218, 201–214.

Meibom, A., Cuif, J.-P., Hillion, F., Constantz, B.R., Juillet-Leclerc, A., Dauphin, Y., Watanabe, T., Dunbar, R.B., 2004. Distribution of magnesium in coral skeleton. Geophys. Res. Lett. 31.

Odum, H.T., 1951. Notes on the strontium content of Sea Water, Celestite Radiolaria, and Strontianite Snail Shells. Science 114 (2956), 211–213.

Plummer, L.N., Busenberg, E., 1987. Thermodynamics of aragonite-strontianite solid solutions: results from stoichiometric solubility at 25 and 76°C. Geochim. Cosmochim. Acta 51, 1393–1411.

Rodriguez-Cruz, S.E., Jockusch, R.A., Williams, E.R., 1999. Binding energies of hexahydrated alkaline earth metal ions, $M^{2+}(H_2O)_6$, M = Mg, Ca, Sr, Ba: evidence of isomeric structures for magnesium. J. Am. Chem. Soc. 121 (9), 1986–1987.

Schultze-lam, S., Beveridge, T.J., 1994. Nucleation of celestite and strontianite on a cyanobacterial S-layer. Appl. Environ. Microbiol. 60 (2), 447–453.

Speer, 1983. Crystal chemistry and phase relations of orthorhombic carbonates. In: Reeder, R.J. (Ed.), Reviews in Mineralogy: Carbonates –Mineralogy and Chemistry, pp. 145–189.

Stoll, H.M., Klaas, C.M., Probert, I., Encinar, J.R., Alonso, J.I.G., 2002. Calcification rate and temperature effects on Sr partitioning in coccoliths of multiple species of coccolithophorids in culture. Glob. Planet. Chang. 34, 153–171.

Tang, J., Köhler, S.J., Dietzel, M., 2008a. Sr^{2+}/Ca^{2+} and $^{44}Ca/^{40}Ca$ fractionation during inorganic calcite formation: I. Sr incorporation. Geochim. Cosmochim. Acta 72, 3718–3732.

Tang, J., Dietzel, M., Böhm, F., Köhler, S.J., Eisenhauer, A., 2008b. Sr^{2+}/Ca^{2+} and $^{44}Ca/^{40}Ca$ fractionation during inorganic calcite formation: II. Ca isotopes. Geochim. Cosmochim. Acta 72, 3733–3745.

Tang, J., Niedermayr, A., Köhler, S.J., Böhm, F., Kisakürek, B., Eisenhauer, A., Dietzel, M., 2012. Sr^{2+}/Ca^{2+} and $^{44}Ca/^{40}Ca$ fractionation during inorganic calcite formation: III. Impact of salinity/ionic strength. Geochim. Cosmochim. Acta 77, 432–443.

Vollstaedt, H., Eisenhauer, A., Wallmann, K., Böhm, F., Fietzke, J., Liebetrau, V., Krabbenhöft, A., Farkaš, J., Tomašových, A., Raddatz, J., Veizer, J., 2014. The Phanerozoic $\delta^{88/86}Sr$ record of seawater: New constraints on past changes in oceanic carbonate fluxes. Geochim. Cosmochim. Acta 128, 249–265.

Watson, E.B., 2004. A conceptual model for near-surface kinetic controls on the trace element and stable isotope composition of abiogenic calcite crystals. Geochim. Cosmochim. Acta 68, 1473–1488.